ELECTRONIC SUPPLEMENTARY INFORMATION

Transport, Trapping, Triplet Fusion: Thermally Retarded Exciton Migration in Tetracene Single Crystals

Dominik Muth[1], *Sebastian Anhäuser*[2], *Daniel Bischof*[2], *Anton Krüger*[1], *Gregor Witte*[2*]

and Marina Gerhard[1*]

*marina.gerhard@physik.uni-marburg.de

[1]Departmentof Physics and Material Sciences Center, Semiconductor Spectroscopy Group, Philipps-Universität Marburg, Renthof 7a, 35032 Marburg, Germany

[2]Department of Physics and Material Sciences Center, Molecular Solids Group, Philipps-Universität Marburg, Renthof 7, 35032 Marburg, Germany

Contents

1. Spatial calibration of the streak camera data

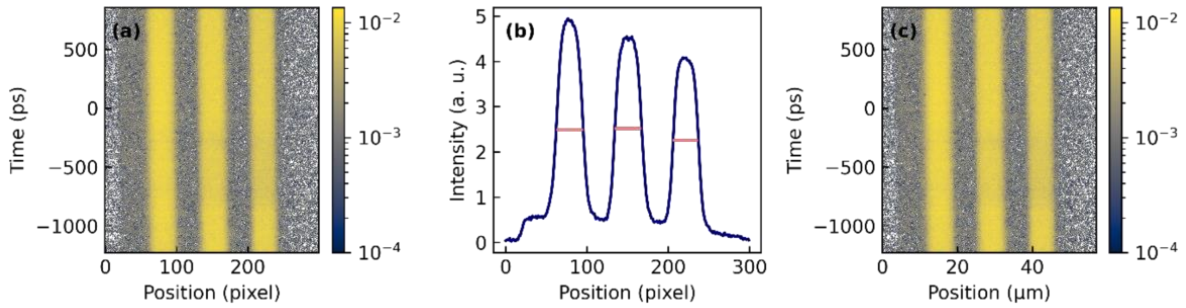

Figure S1: Spatial calibration of streak camera data. (a) 2D plot of three imaged reference lines with a width of 6.3 µm recorded in the synchroscan mode. (b) Extracted intensity profiles (blue) with FWHM (red) and (c) 2D plot of imaged lines with corrected x-axis displaying real distances.

In order to determine the size of the excitation profile, it was necessary to calculate the correlation between the actual size of an object and the size it was displayed as in the streak camera. In order to achieve this, lines with known thickness on a resolution test target (Thorlabs NBS 1952) were imaged with the white light of a tungsten halogen lamp (**Figure S1a**). The spatial image was captured by the streak camera and the FWHM of the lines (**Figure S1b**) was determined. Afterwards a correlation factor between the horizontal units output by the camera and real distances in µm was calculated. This was achieved by dividing the known line thickness by the measured FWHM signal, which was given in pixel. By multiplying the x-scale of the spatial data with this factor, we were able to determine the size of the captured profiles in the MSD measurements.

From the edges of the lines of the resolution target (distance over which the reflected intensity rises to half of the maximum value), the spatial resolution of the setup was determined to be 1.1 µm.

2. Out of plane XRD-measurements

To characterise the crystalline orientation and order of the differently prepared TET single crystals they were analysed by specular X-ray diffraction measurements. The out-of-plane diffractograms were recorded in Bragg-Brentano geometry using a Bruker D8 Discover diffractometer equipped with a Göbel mirror yielding monochromatized Cu Kα radiation (λ = 1.542 A) and a sensitive one-dimensional LynxEye silicon strip detector. As depicted in **Figure S2** both preparation methods yield (001)-oriented crystals of the bulk structure, evidenced by the comparison with the calculated powder diffractogram. However, the DSC samples reveal lower intensities of the higher order (00n) reflections relative to the (001) reflection, thereby indicating their lower crystalline order.

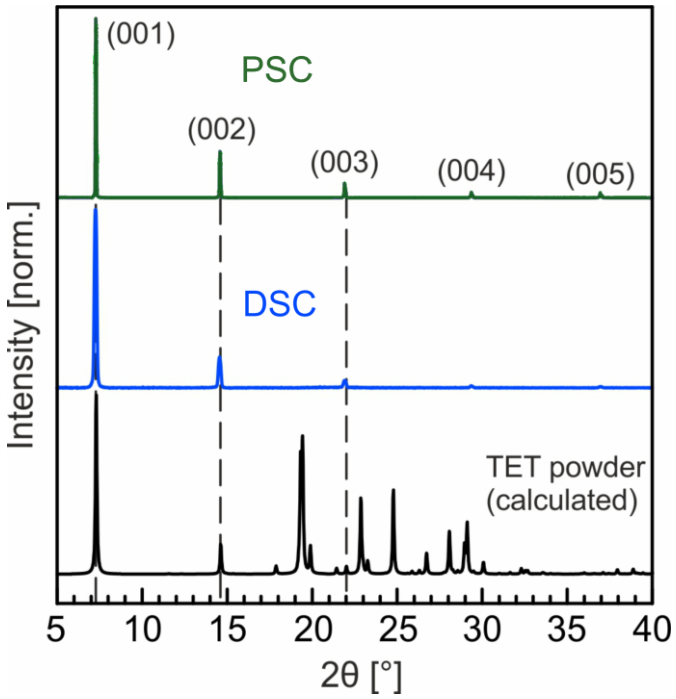

Figure S2: Specular X-ray diffractograms of PSC and DSC TET-crystals that are compared with a powder diffractogram calculated from the known tetracene bulk crystals structure. [S1]

3. Thickness dependent PL shift

The highest energy emission band of TET at approx. 2.32eV (530nm) has been attributed to the zero-phonon-line of the free exciton emission. In order to support this assignment, we show the comparison between unpolarised UV/Vis absorption and PL spectra of a thin (30 nm) polycrystalline TET film at room temperature in **Figure S3**. The film was deposited onto a KCl(100) surface, yielding a smooth morphology where the real thickness matches the nominal thickness very precisely as shown in a previous study,[S1] making it ideal for optical spectroscopy.

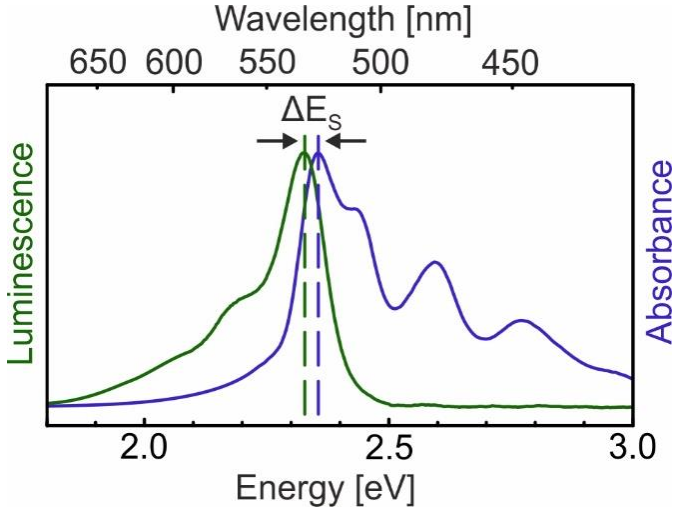

Figure S3: Comparison between UV/Vis absorption and PL spectra of a polycrystalline TET film on KCl(100) with a nominal thickness of 30 nm, recorded for an excitation wavelength of λ_{ex} = 360-380 nm. The small Stokes shift of ΔE_s = 30 meV is highlighted.

The spectra reveal a very small Stokes shift of approx. ΔE_s = 30 meV between the lowest energy absorption and the highest energy emission band. In fact, there is a significant spectral overlap between the two peaks. On the one hand, this proves that the emission at 2.32 eV can indeed be assigned to the zero-phonon-line. On the other hand, the spectral overlap gives rise to artefacts, which occur when taking spectra of samples with different thicknesses. When measuring the absorbance, photons that were absorbed within the overlap region can be re-emitted again at the same wavelength so that the spectrometer actually detects a reduced absorbance. Similarly, during PL measurements the emitted photons can get re-absorbed, thereby reducing the detected intensity in this spectral region. Since these processes are more likely to happen the longer the optical path through the medium is, thicker samples suffer more from these artefacts. This has also been analysed in previous work quantitatively.[S2]

In this study, the thickness-effect of the TET PL becomes evident when comparing the spectra of the PSC and DSC samples. Since the PSC is much thicker (> 70 µm) than the DSC (< 1 µm), the peak position of the highest energy emission in the PSC undergoes a comparably larger shift towards lower energies. This is due to the fact that the re-absorption of the higher energy flank of the peak is more pronounced because of the higher thickness. To quantify this apparent peak shift, we measured PL

spectra of TET films on KCl(100) surfaces as a function of film thickness, which can be seen in **Figure S4**. By increasing the thickness up to 2 µm, the peak maximum shifts by almost 30 meV. It is worth mentioning here, that the thickness-effect in PL spectra taken in reflection geometry also critically depends on the excitation wavelength and density, because those determine the penetration depth and therefore the length of the optical path which emitted photons have to travel through the medium before being detected by the spectrometer.

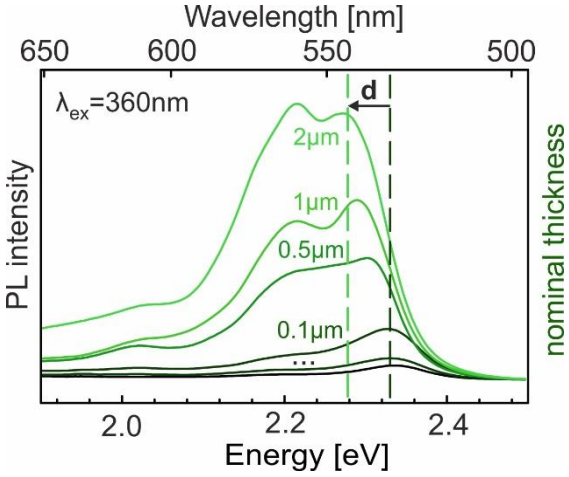

Figure S4: PL spectra of polycrystalline TET films with varying thickness on KCl(100). Due to re-absorption effects, the peak position of the highest energy emission undergoes an apparent shift of 30 meV with increasing thickness d.

4. The yellow emission band

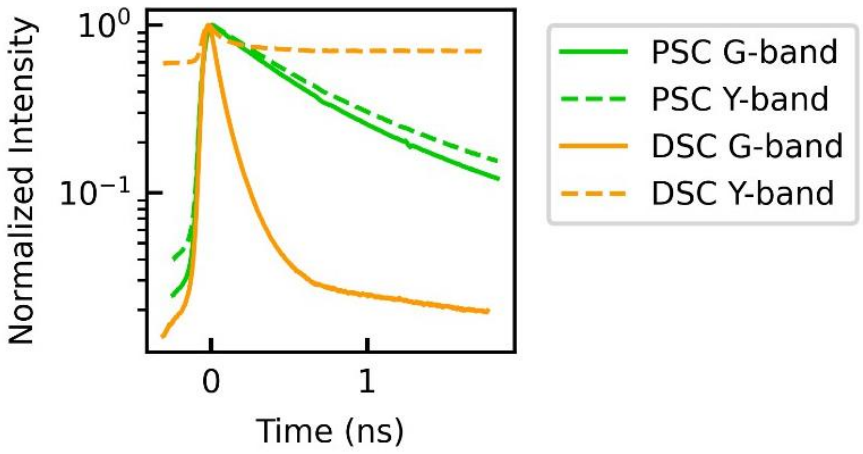

Figure S5: Comparison of the transients of the green (G, 525-545 nm) and the yellow (Y, 565-585 nm) emission band for the PSC and DSC sample at a temperature of 80 K

When comparing the main emission bands for the PSC and DSC sample at low temperatures, as also shown in Figure 2 in the main text, the difference in their lifetimes becomes apparent. To further emphasize this difference, the transients for said bands were calculated by integrating over the spectral range from 525 to 545 nm for the green and 565 to 585 nm for the yellow emission band, referred to as G- and Y-band in the following. The transients shown in **Figure S5** further highlight the similar decay behaviour for the PSC sample bands, indicating that the Y-band in this case seems to originate from a sideband of the singlet emission. In contrast, the Y-band in the DSC sample is much longer lived than the corresponding G-band, which exhibits a substantially lower lifetime than the same species does in its pristine counterpart, see **Table S1**. This in turn also seems to suggest the presence a trapping mechanism, which depopulates the singlet species. In combination with the temperature induced relative intensity shift between both bands, as seen in the spectra of Figure 1f in the main text, it seems likely that this trapped species is responsible for the Y-band emission of the DSC sample. The fact that this longer-lived emission overlaps spectrally with the sideband of the exciton emission might also explain why we observe a slightly longer lifetime of the Y-band in the PSC compared to the G-band, since those defects might still be present in the PSC sample, just to a lesser degree.

Table S1: Decay constants for the two high energy bands of the PSC and DSC sample. The first 3 parameters were obtained from the measured data. This was however not possible for the yellow DSC band, since its decay was much longer than our observable timeframe. The software Glotaran [S3] was used instead to fit its transient with a biexponential function to obtain the decay constant for the longer-lived species.

Description	Decay constants
PSC G-band	1.5×10^9 s^{-1}
PSC Y-band	1.3×10^9 s^{-1}
DSC G-band	1.2×10^{10} s^{-1}
DSC Y-band	1.0×10^8 s^{-1}

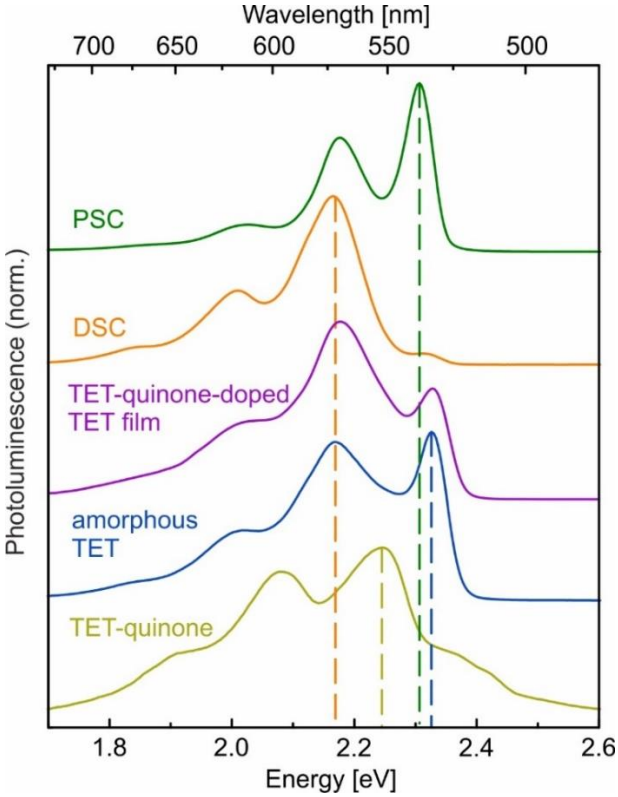

Figure S6: Comparison of the steady state PL spectra of pristine and defective TET single crystals (PSC, DSC), amorphous TET and TET-quinone films as well as polycrystalline TET-quinone doped TET films, recorded at 100 K.

To identify the origin of the low temperature yellow emission band of the DSC samples, the PL characteristics of additional molecular films were examined. First, we analyzed amorphous TET films which were prepared by depositing TET films onto quartz glass substrates at cryogenic temperatures and measuring their PL signature while keeping the films at low temperature to suppress any thermally induced recrystallization. The PL signature of the amorphous TET film essentially resembles that of the PSC film and only shows broader emission peaks as well as a slightly upshifted zero-line, which can be explained by the absence of Davydov splitting, while the PL of the PSC occurs at the lower energy Davydov component.[S4] OMBD grown TET-quinone (5,12-Naphthacenequinone, Sigma Aldrich, purity > 97%) films exhibit the highest energy PL band around 2.25 eV as well as lower energy vibrational replica. While these films reveal a yellowish emission, its spectral signature barely changes with temperature and does not match the PL of the DSC sample. With such an approach, however, one must keep in mind that a partially oxidized sample is not a pure quinone film and that the quinones rather act as dopants embedded in TET. To mimic such a doping effect in a homogenous mixture and to avoid phase separation between TET and quinone, additional (polycrystalline) films were prepared by drop-casting from a toluene solution of TET and TET-quinone. The rapid evaporation of the solvent yields well intermixed solids, of which the PL signature at low temperature is very similar to that of the DSC samples.

5. PL of Polycrystalline TET films

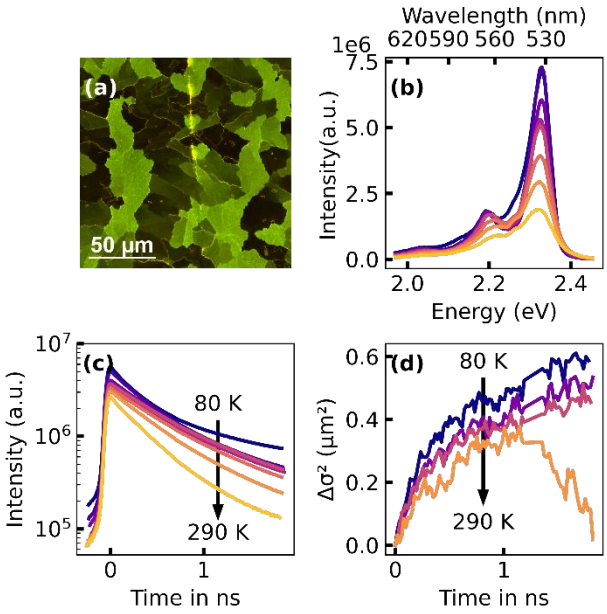

Figure S7: (a) PL-micrograph of a poly-crystalline thin TET film, (b) temperature dependent luminescence spectra and (c) transients. Panel (d) shows the mean squared displacement of the PL profile as function of time.

In addition to the TET single crystals, for which the experimental results are presented in the main paper, also polycrystalline TET films were investigated. Exemplary results are summarized in **Figure S7**. The TET films with a thickness of about 1 µm were deposited via organic molecular beam deposition technique onto freshly cleaved KCl(100) single crystal slices. Since such TET films are epitaxially ordered on KCl(100),[S2] they adopt a rather uniform thickness with crystalline domains extending over 10-20 µm, as seen in the polarized PL micrograph (cf. **Figure S7a**). The sample exhibits greenish luminescence similar to the one of the PSC sample which is complemented by the absence of a yellow emission band in the emission spectra (**Figure S7b**). Accordingly, the time resolved emission (**Figure S7c**) also reveals mostly mono-exponential transients. The MSD measurements (**Figure S7d**) show a similar temperature dependence as the PSC at later times as well, with a positive slope at 80 K and a negative one at room temperature. The observed slope during the first 150 ps is, however, considerably lower than in the PSC and more comparable with the DSC sample, see **Table S2.** Since, according to our model, this initial broadening of the profile is mainly determined by the singlet exciton diffusion, we can assume a lower effective singlet diffusion coefficient in the polycrystalline sample compared to the single crystals, which might be caused by the presence of grain boundaries hampering the diffusion process.

Table S2: Effective Diffusion coefficients from 0 to 0.27 ns for the PSC, DSC and polycrystalline sample at 80K

PSC	DSC	Polycrystalline
11.0 +/- 3.0 cm²/s	7.0 +/- 0.8 cm²/s	6.9 +/- 0.4 cm²/s

6. Details of the kinetic model

In order to model the spatiotemporal evolution of the photoexcited populations, we numerically solved the set of two-dimensional rate equations presented in the manuscript (Eqn. 2) for a grid of 101 x 101 datapoints with a cell size of 350 x 350 nm², which is of sufficient size to avoid artefacts arising from excitons diffusing out of the simulated grid. As a first step, it is necessary to realistically estimate the initial population of singlet excitons created through a laser pulse. Therefore, the size of the excitation spot was determined experimentally from the initial excitation profile at t = 0 ps, yielding a spot diameter (FWHM) of 5 µm and the corresponding steady state excitation power P_{cw} was 25 µW (measured with a Thorlabs PM100D power meter with attached S120VC sensor). Considering the laser repetition rate f_{rep} of 80 MHz and the excitation wavelength λ_{ex} of 460 nm (for more details regarding the laser system see main text) we calculate the number of photons provided per laser pulse:

$$N = \frac{P_{cw} \cdot \lambda_{ex}}{f_{rep} \cdot h \cdot c}$$

We assume that the excitation profile and with this the distribution of the initial population is of Gaussian shape:

$$g(x,y) = A_0 \exp\left(-\frac{x^2 + y^2}{2\sigma^2}\right)$$

For our simulations, we further consider a volume of dz = 100 nm thickness. With the absorption coefficient α_{TET} of approx. 3.5 µm^{-1}, see Ref. S2, we can now calculate an initial excitation density profile (with the unit excitons per volume), which is normalized such that the area integral over $N_{S,0}(x,y)$ yields the number of photons absorbed in the considered volume:

$$N_{S,0}(x,y) = N \cdot (1 - \exp(-\alpha_{TET} \cdot dz)) \cdot g(x,y)$$

The resulting profile is plotted in Figure 5b in the main text. This profile serves as a starting point for a step-by-step solution of the kinetic model. The different sub-populations (free singlets, triplets and trapped excitons) were modelled in time steps Δt of 2 ps and the luminescence of the free singlet PL_S and the trapped PL_{Trap} species in a certain time frame was calculated from these populations via the decay rates k_0 (radiative rate of singlets) and $k_{trapdec}$, as well as the relative oscillator strength of the emission of the trapped population:

$$PL_S(x,y,t) = N_S(x,y,t) \cdot k_0 \cdot \Delta t$$

$$PL_{Trap}(x,y,t) = N_{Trap}(x,y,t) \cdot k_{trapdec} \cdot \alpha \cdot \Delta t$$

7. Checking for singlet annihilation effects

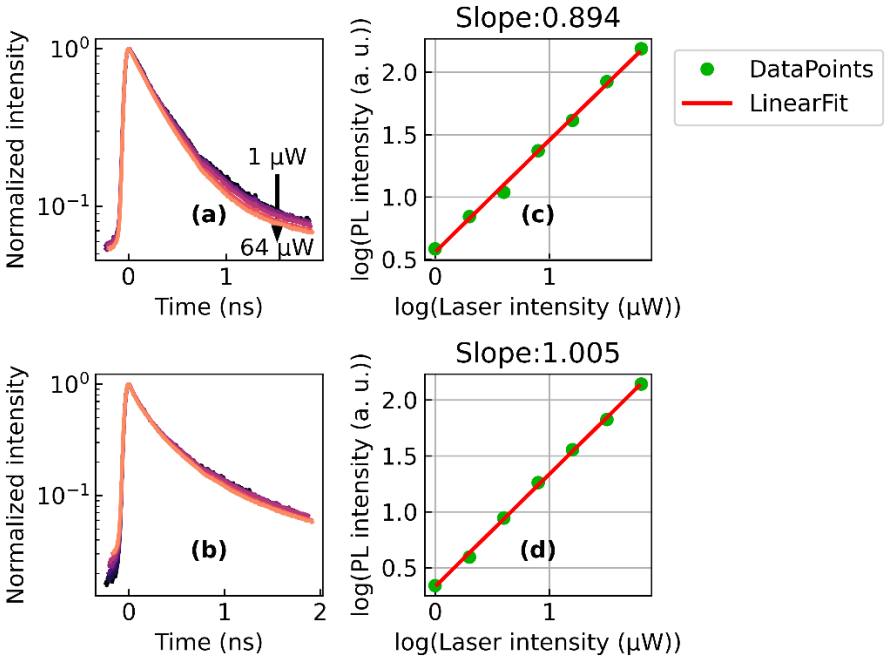

Figure S8: Power series. Normalized transients for the (a) PSC and (b) DSC sample, which were excited with powers ranging from 1 µW (blue curve) to 64 µW (yellow curve). Corresponding integrated luminescence signals for (c) PSC and (d) DSC are plotted against the excitation power. Both axis values are logarithmized and linearly fitted in order to check for non-linear behaviour. Assuming a power law for the PL intensity as function of excitation power, i.e. $I_{PL} \propto P^{\alpha}$, a slope α=1 indicates a linear interrelation, whereas α<1 denotes a sublinear increase of the PL intensity with increasing excitation power, which is indicative for an onset of nonlinear processes, i.e. annihilation effects at higher powers.

In order to test whether exciton-exciton annihilation effects have an influence on our experimental results, a power series has been conducted at room temperature for the PSC and DSC sample, in which the excitation power was increased from 1 to 64 µW. Both sets of transients (**Figure S8a,b**) show no significant deviations in the early time regime around 200 ps, were singlet annihilation events would be expected, thus a significant contribution of these effects to the measured data obtained with an excitation power of 25 µW can be ruled out. There is, however, a deviation in the signals of the PSC sample at later times (**Figure S8a**), starting from 700 ps. The luminescence decay gets slightly faster with increasing excitation densities, which could originate from to the increased contribution of singlet-singlet or singlet-triplet annihilation, which most prominently influences the later time regime of the PSC sample. This might also be the reason why a slightly sub-linear increase of the PL intensity with increasing excitation power is observed for this sample (**Figure S8c**), after the initially excited singlets have decayed. The mentioned deviations in the transients are almost absent in the DSC sample (**Figure S8b**), which also shows a linear behaviour when it comes to the relation of excitation power and luminescence yield (**Figure S8d**). It can therefore be assumed, that at the employed laser power of 25 µW no major Auger-like processes contribute to the luminescence signal of both samples.

8. Comparing measured and fitted curves

In order to fit the measured MSD data to the employed model, the parameters were varied such that the fit would most accurately match both the measured slopes of the MSD and the transients at the same time. From fitting only, the MSD data on the other hand, it became clear that the resulting fit parameters would model the MSD profiles somewhat accurately but failed to simultaneously recreate the shape of the measured transients, see **Figure S9**. A comparison between the experimental data and the final fits is shown in **Figure S10** for the PSC and in **Figure S11** for the DSC sample.

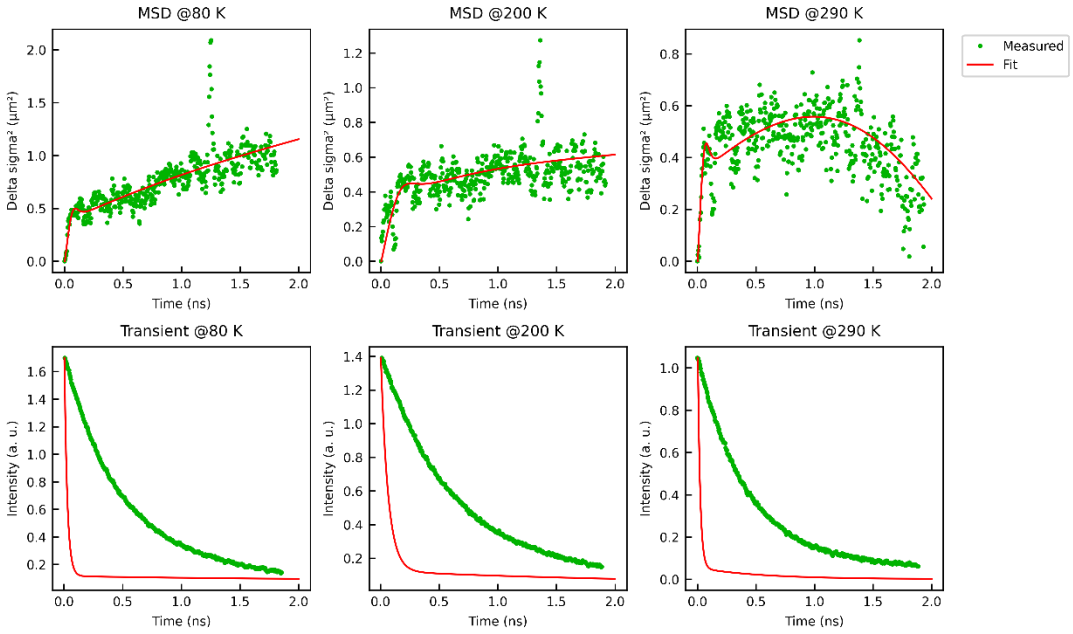

Figure S9: ”Misfits” of the data recorded for the PSC sample, where only the MSD curves were fit, leading to an overestimation of the PL decay.

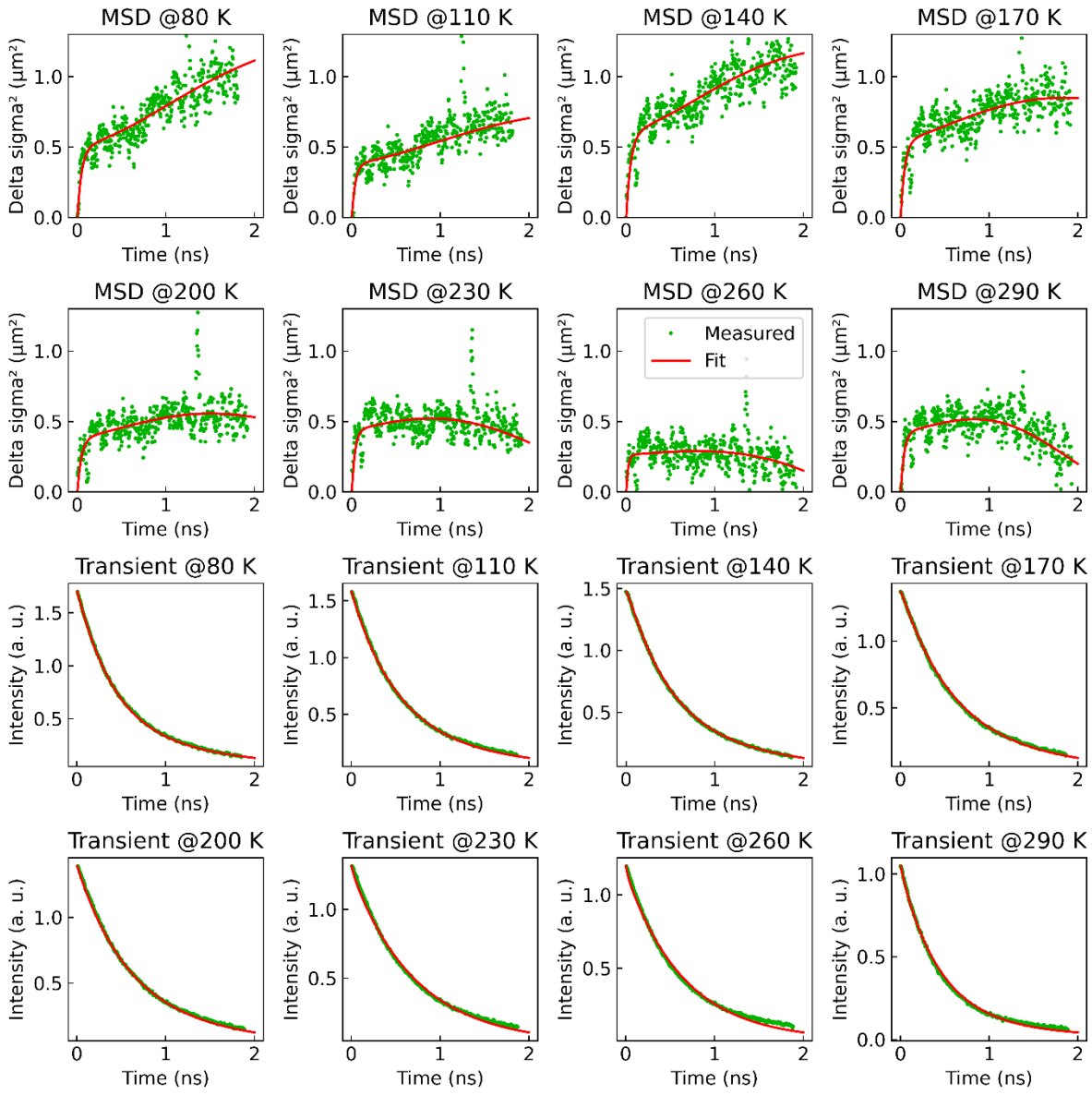

Figure S10: Comparison of measured and fitted data for the MSD curves and the PL transients of the PSC sample.

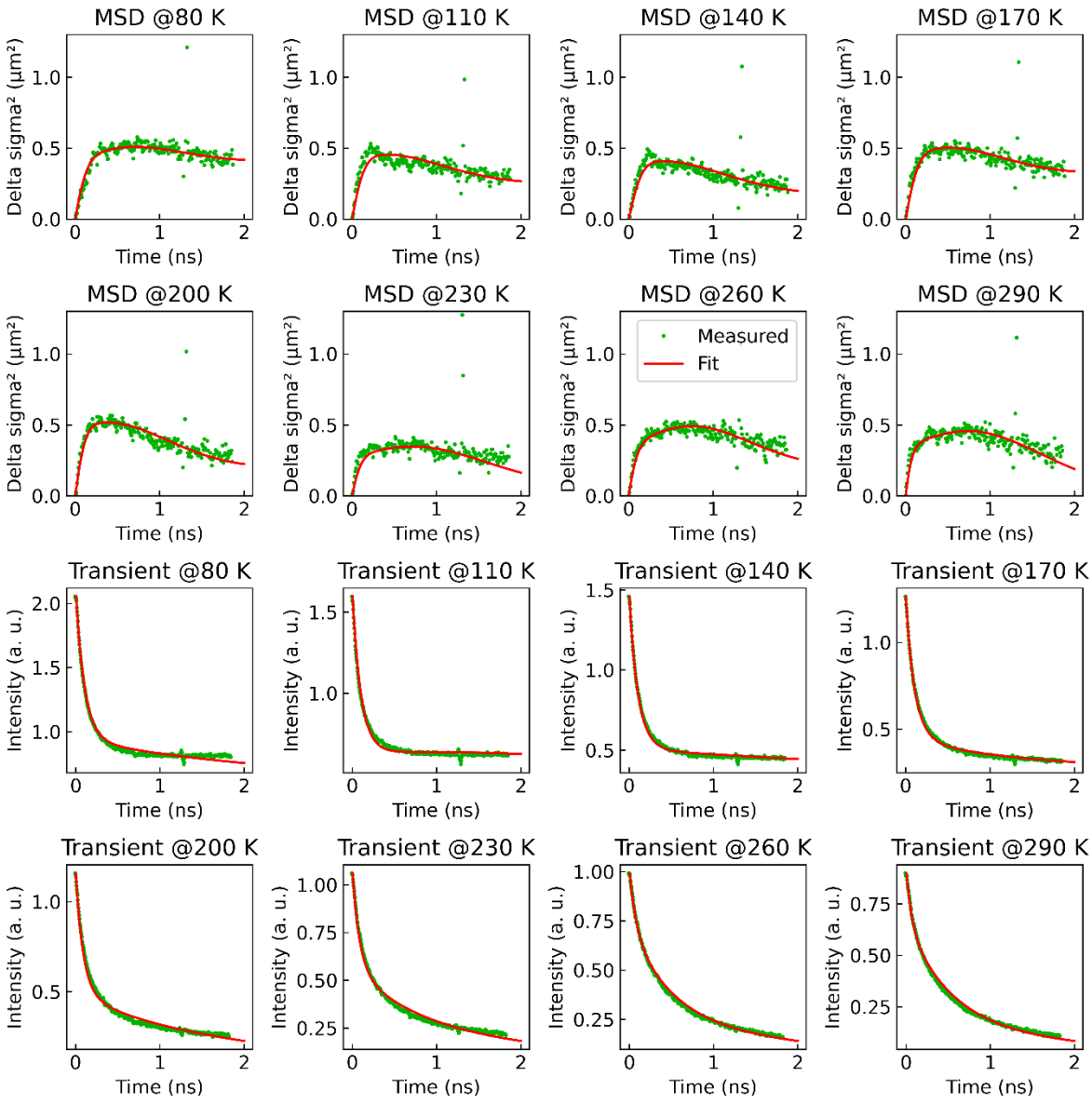

Figure S11: DSC: Comparison of measured and fitted data for the DSC sample.

9. Trap related rate constants

The temperature dependent trapping rates k_{trap}, the decay rates from those trapped exciton states $k_{trapdec}$ and the oscillator strength of the trapped populations α obtained from our fits are summarized in **Figure S12**. As discussed in the main text, surprisingly, also the data for which no yellow emission band is observed, i.e. the data recorded for the PSC sample and the DSC sample at elevated temperatures, can only be modelled by assuming a delayed emissive population subset, potentially related to rather localized excitons. These singlets with the same emission signature as the PL at early times after excitation would have to be generated and/or converted into triplets with differing rate constants to explain this behaviour, suggesting that TTA, singlet fission or fusion might not be single constants but potentially rather a distribution depending on factors such as crystal structure and temperature.

Another aspect to note is the pronounced drop of the oscillator strength of the delayed PL for the DSC sample in **Figure S12b**, which coincides with a sudden rise of the trapping rate of the same sample when increasing the temperature from 170 to 200 K. When comparing this behaviour to the spectral evolution of both samples with temperature shown in Figure 1d,f, this change might be caused by a change of the dominant delayed emitting species. At 80 K, the yellowish PL of trapped excitons dominates the DSC spectrum, whereas above 200 K the PL of free excitons dominates the emission of the PSC and the DSC sample.

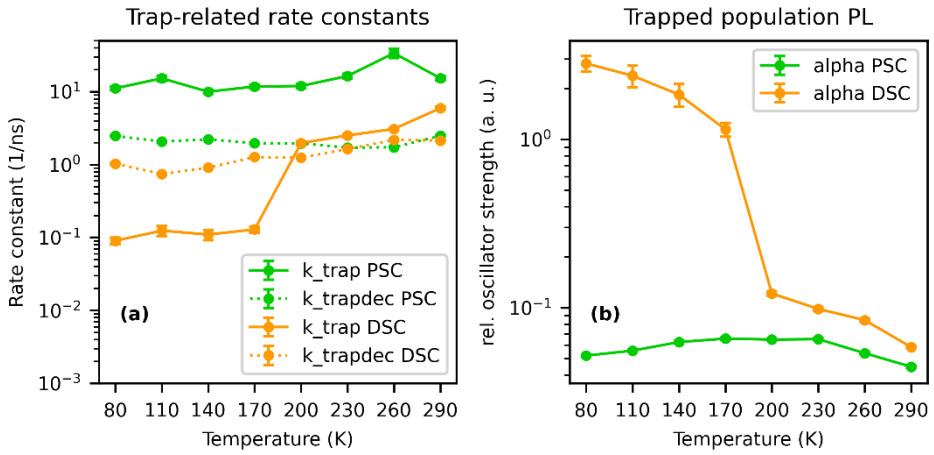

Figure S12: Trap related rate constants obtained from the fitting routine against temperature, k_{trap} and k_{detrap} (a) and the relative oscillator strength α of the trapped population emission (b) for PSC and DSC sample

10. Importance of a delayed species

As can be seen in **Figure S10** and **Figure S11**, the model with the given parameters is able to reproduce the results of the measurements quite well. During the development it became apparent, that even in the PSC sample a single emitting species was unable to explain the measured diffusion behaviour as well as the transients, see the failed fit attempts in **Figure S13** and **Figure S14**. The singlet population simply would decay too quickly to emit enough PL over time to explain the gradual decay of the observed transients.

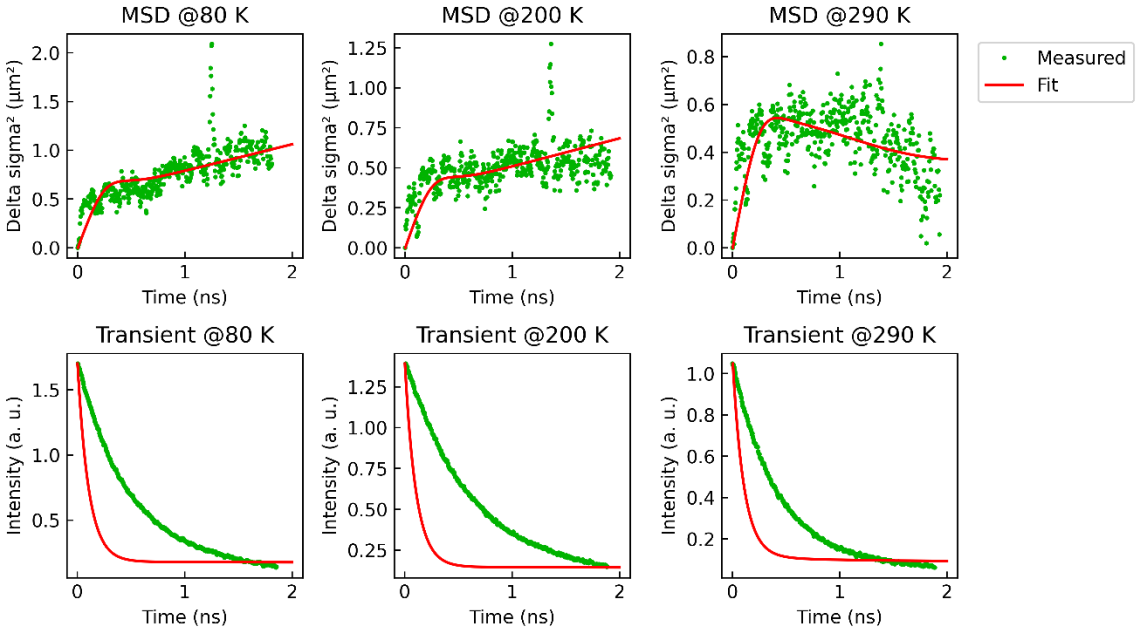

Figure S13: Fit attempts with a non-emitting delayed species for different temperatures ($\alpha = 0$) for the PSC sample.

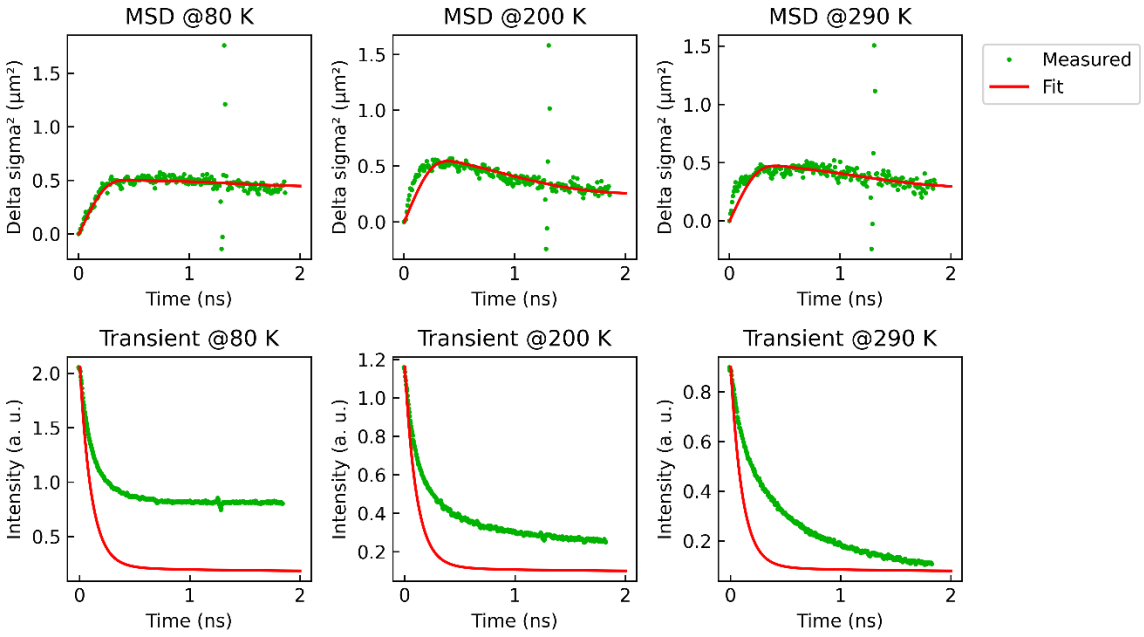

Figure S14: Fit attempts with a non-emitting delayed species for different temperatures ($\alpha = 0$) for the DSC sample.

11. Fluence dependent diffusion measurements and simulations

In order to determine the impact of fluence on the diffusion behaviour of our samples, we conducted a power series at room temperature for both the PSC and DSC sample, during which the excitation power was continuously doubled from 1 to 64 µW for each power step. The series was not extended to higher fluences in order to not permanently damage the delicate organic crystals.

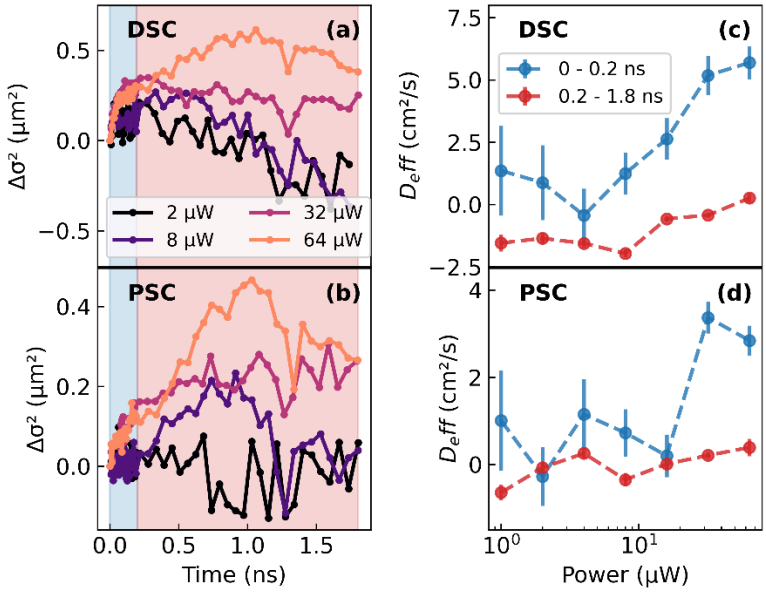

Figure S15: MSD-curves (left) recorded at 290K with varying excitation powers for DSC (a,c) and PSC (b,d) samples. Effective diffusion coefficients (c,d) were calculated for the short (0-0.2 ns) indicated as blue and long (0.2-1.8 ns) time regime indicated as red.

In addition, simulations were carried out, in which the laser power was matched to the values of the measurement, the results are shown in **Figure S16**.

As can be seen from the results in **Figure S15** increasing the power above 8 µW seems to steadily increase the effective diffusion constants, especially in the DSC sample. This runs counter to the simulated curves, in which we observe a steady diffusion in the first 0.2 ns but a decrease of the diffusivity at later times, when increasing the fluence. A reason for this discrepancy could be the relaxation of excitons into free tail states with a lower mobility, which the simulation is unable to account for, whereas at higher fluences, excitons can propagate further because tail states are saturated and thus the behaviour of the MSD is closer to that predicted by our model.

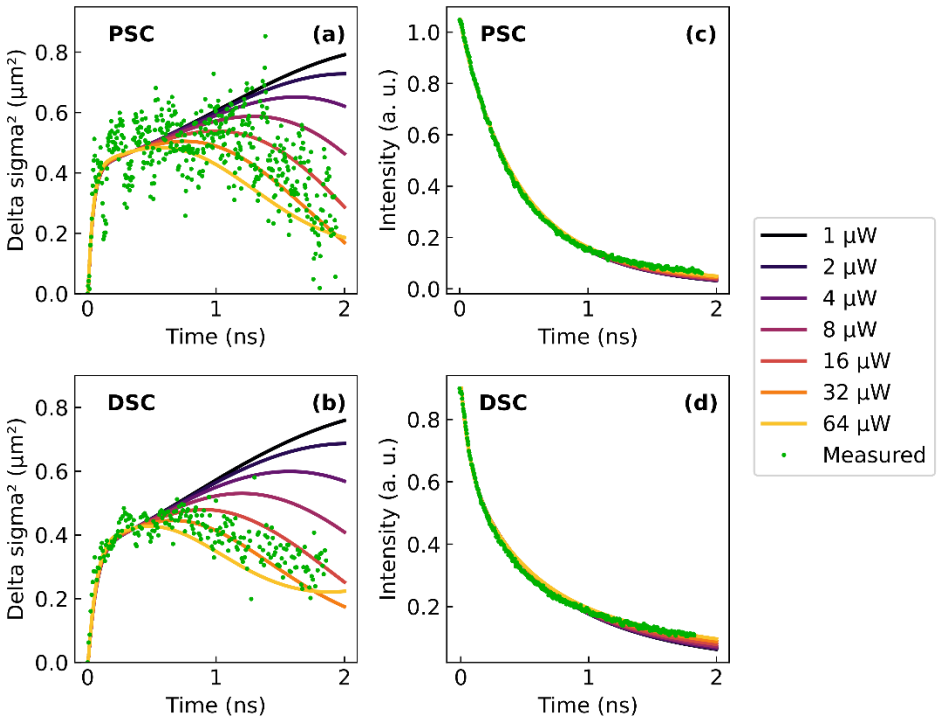

Figure S16: Simulated slopes of the MSD at room temperature for different fluences for the PSC (a) and the DSC sample (b). Green dots represent experimental data recorded at a fluence of 25 µW. Simulated and measured decay curves are presented in (c,d).

References

[S1] D. Holmes, S. Kumaraswamy, A. J. Matzger and K. P. C. Vollhardt, *Chem. - Eur. J.*, 1999, **5**, 3399.

[S2] A. M. Valencia, D. Bischof, S. Anhäuser, M. Zeplichal, A. Terfort, G. Witte and C. Cocchi, *Electronic Structure*, 2023, **5**, 033003.

[S3] J. J. Snellenburg, S. Laptenok, R. Seger, K. M. Mullen and I. H. M. van Stokkum, *J. Stat. Softw.*, 2012, **49**, 1–22.

[S4] J. J. P. Thompson, D. Muth, S. Anhäuser, D. Bischof, M. Gerhard, G. Witte and E. Malic, *Natural Sciences*, 2023, **3**, e20220040.